Thermochimica Acta, 228 (1993) 155–171
Elsevier Science Publishers B.V., Amsterdam

Spectroscopic and microscopic investigations of the thermal decomposition of nickel oxysalts. Part 1. Tetrahydroxy nickel carbonate

Seham A.A. Mansour

Chemistry Department, Faculty of Science, Minia University, El-Minia (Egypt)

(Received 16 February 1993; accepted 18 March 1993)

Abstract

A study of the thermal decomposition of tetrahydroxy nickel carbonate $NiCO_3 \cdot 2Ni(OH)_2 \cdot 4H_2O$, was performed by thermogravimetric analysis (TGA), differential thermal analysis (DTA) and differential scanning calorimetry (DSC) under non-isothermal conditions in dynamic atmospheres of dry air or nitrogen, at different heating rates. Non-isothermal kinetic and thermodynamic parameters were calculated from the effect of heating rates on the maximum temperature of TG and DTA peaks, as well as from the recorded DSC data, using the Ozawa method. The parent material, the intermediates and the final product were characterized by means of infrared spectroscopy and X-ray diffractometry (XRD). The decomposition of tetrahydroxy nickel carbonate commenced through two steps (dehydration and decomposition). The dehydrated intermediate from the first step was found to contain an XRD detectable NiOOH phase. The morphological changes throughout the decomposition course were examined by scanning electron microscopy (SEM) and found to be in accord with the thermal analysis. A reaction pathway is proposed.

INTRODUCTION

Metal hydroxy carbonates (basic metal carbonates) are important in the wet corrosion of metals, weathering of materials, and as raw materials in metal refining and ceramic processing, etc. [1]. Many basic nickel carbonates are known, some of which are hydrated, though the water is usually combined in at least two different ways [2]. The thermal decomposition of basic nickel carbonates has been the subject of several studies [3–5]; they are of particular interest, since several nickel catalysts are prepared by decomposition of these carbonates and reduction of the decomposition products [6]. Furthermore, these carbonates are parents of the oxidant nickel(II), which is frequently used as a catalyst for important catalytic reactions [4].

The thermal decomposition of basic nickel carbonates has been reported as completing in the temperature range 420–500°C depending on the structure and/or the experimental conditions [5]. Dollimore and Taylor [4]

found that the mechanism of decomposition of a series of pure carbonates, including basic nickel carbonate, obeys first order kinetics.

Non-isothermal kinetic studies of these carbonates have been carried out from a single TG-curve using different mathematical treatments [7, 8]. It has been stated [9] that such treatments, which involve very accurate statistical and mathematical methods, result in large errors. This may explain the variation in the reported kinetic parameters of tetrahydroxy nickel carbonate (THNC) [3, 4, 9]. Hence, it seemed most desirable to adopt the method proposed by Ozawa [10] for the decomposition of THNC, where the kinetic parameters are calculated from mathematical analysis of series of TG, DTA and DSC curves obtained at different heating rates.

Galwey [11] pointed out that the interpretation of kinetic data should be supported by all other available and relevant evidence; also the chemical approach should be considered in the reactions involving solids. Therefore, for the sake of exploring the decomposition course of THNC, the structural transformations and identification of the intermediates have been examined via X-ray diffractometry and infrared spectroscopic analyses. The data was supplemented by microscopic observations of the morphological changes throughout the course of decomposition.

EXPERIMENTAL

Materials and techniques

Tetrahydroxy nickel carbonate used was an AR grade (>99% pure) Merk product with the formula $NiCO_3 \cdot 2Ni(OH)_2 \cdot 4H_2O$. Calcination was carried out for 2 h in a still atmosphere of air at temperatures chosen on the basis of thermal analysis results (see below). The calcinated solid products were kept dry over P_2O_5 for further analysis.

Thermogravimetric (TG), differential thermal analysis (DTA) and differential scanning calorimetric (DSC) analyses were performed with an automatically recording Shimadzu Unit (Model 30H; Kyoto, Japan).

TG and DTA curves were recorded on heating samples (≈10 mg size) up to 600°C at four different heating rates ($\theta = 2$, 5, 10 and 20 K min^{-1}) in a dynamic atmosphere of dry air (30 cm^3 min^{-1}). Highly sintered α-Al_2O_3 was used as a reference material for DTA measurements. Separate TG and DTA experiments were carried out in a dynamic atmosphere of dry nitrogen (30 cm^3 min^{-1}) at a heating rate of 10 K min^{-1}. DSC data were recorded over the same range of temperature at different heating rates ($\theta = 2, 5, 10, 20$ K min^{-1}; as for TG and DTA) in a dynamic atmosphere of dry nitrogen (30 cm^3 min^{-1}). The heat of fusion (20.24 J g^{-1}) [12] of specpure indium metal (Johnson Matthey) at 157°C was adopted for the DSC calibration.

DATA ANALYSIS PROCEDURE

Calculation of the kinetic parameters from TG and DTA

From the thermoanalytical curves, the logarithm of heating rates ($\log \theta$) is plotted versus the reciprocal of absolute temperature (T K) at which the sample decomposed to the same amount (TG) accompanying each weight loss of thermal events encountered, or the peak temperature of the DTA curves corresponding to invariant weight processes. The activation energy (ΔE kJ mol^{-1}) was then calculated for each event from the equation [10]

$$\log \theta_1 + 0.4567 \frac{\Delta E}{RT_1} = \log \theta_2 + 0.4567 \frac{\Delta E}{RT_2} \quad (1)$$

where θ_1, θ_2, ... are the heating rates and T_1, T_2, ... are the temperatures determined above, while R is the universal gas constant. Hence, the slope of the straight line is -0.457 ($\Delta E/R$).

Calculation of the frequency factor A min^{-1} was carried out assuming first order kinetics using the equation [10]

$$\log[-\log(1 - C)/T^2] = \log AR/\theta\ \Delta E - \Delta E/2.3RT \quad (2)$$

where C is the fraction decomposed and T is the corresponding temperature in kelvin. The calculated ΔE and A values were used to calculate the reaction rate constant k (min^{-1}) from the Arrhenius equation

$$k = A \exp(-\Delta E/RT)$$

Calculation of the kinetic parameters from DSC data

ΔE, A and k are calculated using the method proposed by Ozawa [10] for DSC measurements at different heating rates. The method has been evaluated for use with industrial materials [13] and is the basis of an ASTM technique developed by committee E 27 on Hazard Potential of Chemicals [14]. A plot of the logarithm of the heating rate θ versus the reciprocal of the absolute peak temperature T gives a straight line with a slope for which the activation energy ΔE is calculated from the equation [10]

$$\Delta E = 2.19R\ \mathrm{d} \log(\theta)/\mathrm{d}(1/T) \quad (3)$$

where R, is the universal gas constant.

The pre-exponential factor A (min^{-1}) and the rate constant k (min^{-1}) at T are obtained from the relations

$$A = (\theta \exp - \Delta E/RT)/RT^2 \quad (4)$$

and

$$k = A \exp(-\Delta E/RT) \quad (5)$$

The enthalpic change ΔH ($J\,g^{-1}$) was directly determined from the DSC data recorded at $10\,K\,min^{-1}$) from the equation [15]

$$\Delta H = 60BCq_m a/m \quad (6)$$

where B is the time base ($min\,cm^{-1}$), C is the cell calibration coefficient, q_m is the Y-axis sensitivity ($J\,s^{-1}\,cm^{-1}$), a is the peak area (cm^2) and m is the sample weight (g). ΔH thus determined was used to calculate the specific heat capacity C_p ($J\,K^{-1}\,g^{-1}$) using the equation $C_p = \Delta H/\Delta T$, where $\Delta T = T_2 - T_1$ and T_1 is the temperature at which the DSC curve begins to leave the baseline, whereas T_2 is the temperature at which the peak lands [16]. Subsequently, the entropy change ΔS ($J\,K^{-1}\,g^{-1}$) was calculated using the relationship $\Delta S = C_p \ln(T_2/T_1)$ [16].

Infrared spectroscopy

IR analysis of THNC and its calcination products were carried out over the frequency range 4000–300 cm^{-1}, at a resolution of 5.3 cm^{-1}, using a model 580B Perkin-Elmer spectrophotometer (UK). Spectra were measured in KBr discs at 1% loading.

X-ray diffractometry

XRD analyses of THNC and its calcination products were carried out by means of a model JSX-60 PA Joel diffractometer (Japan), using Ni-filtered Cu Kα radiation. For identification purposes the diffraction patterns, I/I_0 versus d-spacing obtained were matched with the ASTM standards [17].

Electron microscopy

Samples of THNC and its calcination products were examined in a Jeol 35CF scanning electron microscope. The samples were mounted for viewing and coated with thin layer of gold to render them conducting.

RESULTS AND DISCUSSION

Thermal events encountered throughout the course of decomposition

TG and DTA curves obtained on heating tetrahydroxy basic nickel carbonate (THNC) up to 600°C at different heating rates and in dynamic atmosphere of air (30 $cm^3 min^{-1}$), are shown in Fig. 1. Decomposition

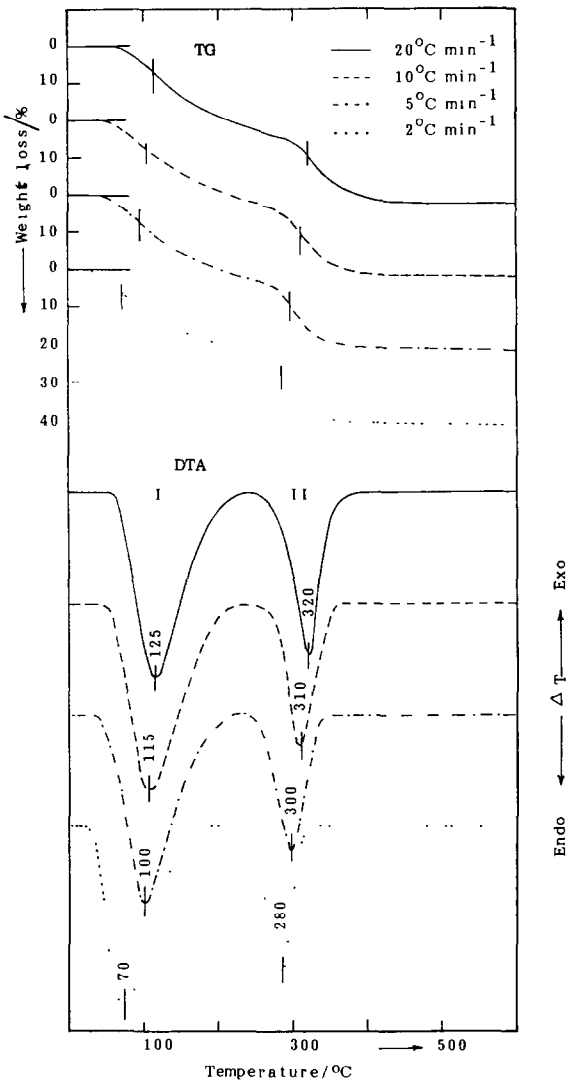

Fig. 1. TG and DTA of THNC at the heating rates indicated and in dynamic atmosphere of air (30 $cm^3 min^{-1}$). Roman numerals I and II indicate locations of the stages encountered.

occurs involving two endothermic processes. The first has a maximum rate between 75 and 115°C (DTA), depending on the heating rate, and is accompanied by a weight loss of 21.3%. This loss is slightly higher than the calculated value for the dehydration of THNC (about 19.9%). The second step, has a maximum rate between 280–320°C (DTA) and brings the total weight loss up to 42%. This is again higher than the calculated value for the decomposition of THNC to NiO. This additional weight loss (≈1.5%) could be due to the presence of adsorbed water. TG curves, in addition indicate that the material loses weight between the first and the second steps, but at a slow rate, at all the heating rates used.

Analysis of the course of thermal events

Figure 2 shows the IR spectra of THNC and its calcination products at 220, 550, 700 and 900°C. Figure 2, curve a displays the IR spectrum of the parent THNC. It exhibits almost all the characteristic absorptions of the carbonate ion (1450, 1070, 830 cm^{-1} [18]), water of crystallization (at 1650 and 800 cm^{-1} [18]) and Ni–O (450 cm^{-1} [18]). The broad band at 3440 cm^{-1}

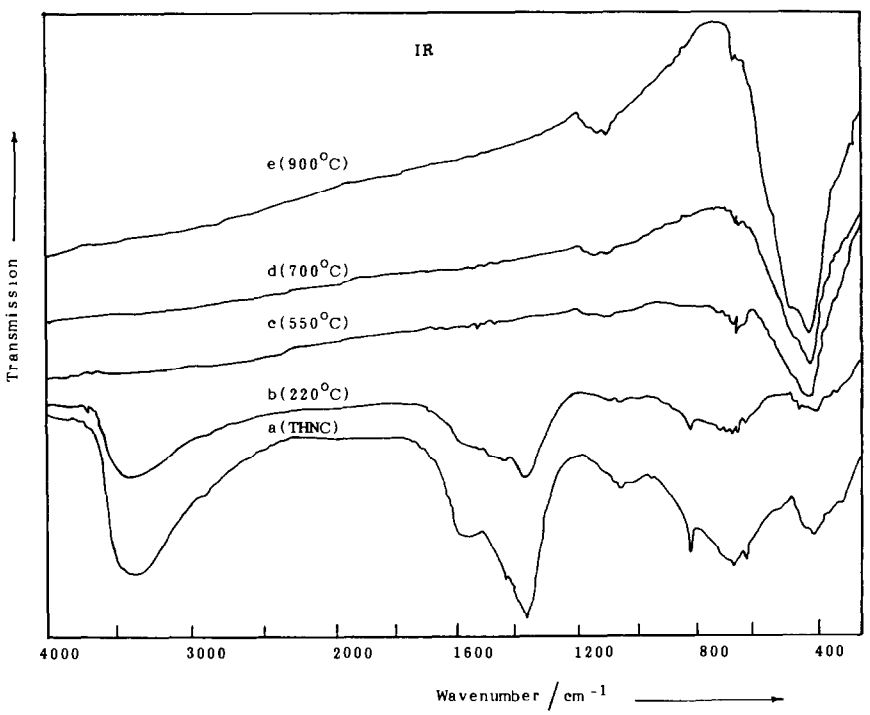

Fig. 2. IR Spectra of THNC (curve a) and its solid calcination products (curves b–e) at the temperatures indicated (resolution 5.3 cm^{-1}).

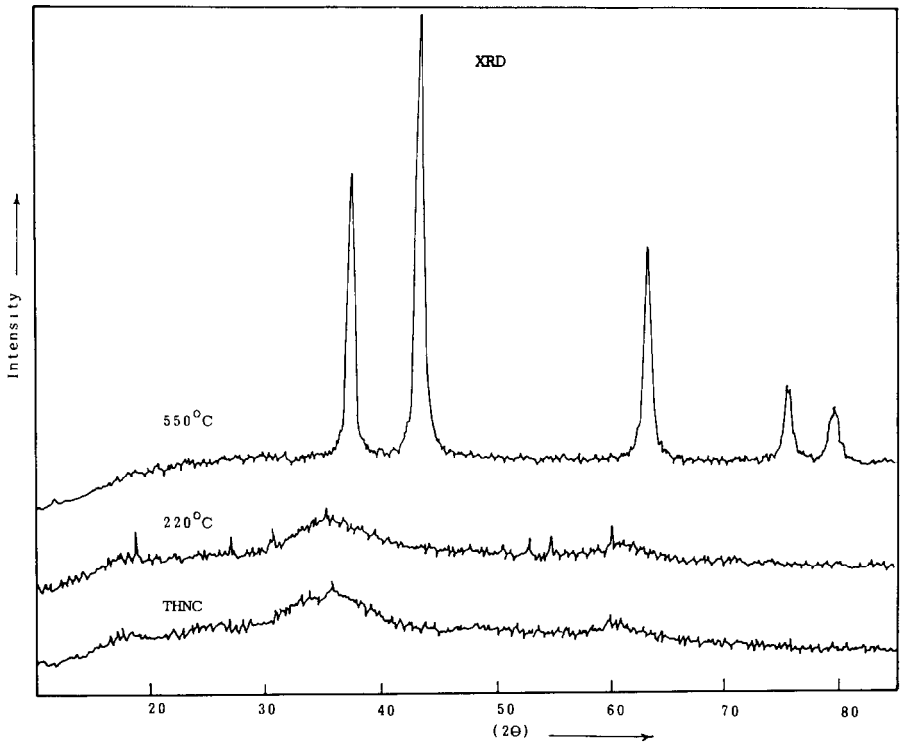

Fig. 3. XRD powder diffractograms of THNC and its solid decomposition products (decomposition temperatures as indicated).

is characteristic of hydrogen bonded OH group [18]. Figure 3 shows XRD results for the parent material and its calcination products. The XRD of the parent THNC (Fig. 3) shows bands at d-spacings typical of $NiCO_3 \cdot 2Ni(OH)_2 \cdot 4H_2O$ (ASTM card no. 16-164) [17]. The diffractogram reveals the low crystallinity of the material.

The IR spectrum of the calcination product at 220°C (i.e. after the commencement of the first thermal event) shown in Fig. 2, curve b displays almost the same absorptions as that of THNC. The spectrum reveals the presence of the hydrogen bonded OH groups (broad band centred around 3440 cm^{-1}) [18], and absorption at (1620 cm^{-1}) characteristic of water. XRD of this calcination product at 220°C (Fig. 3) displays, in addition to THNC, an ill-defined structure with low intensity peaks at d-spacing of 4.67, 3.28, 2.89, 1.7 and 1.68 Å. These peaks are characteristic of the presence of a small portion of NiOOH structure (ASTM card no. 27-956). Apparently, a topochemical decomposition of the nickel hydroxide species of the THNC occurred giving rise to small portions of NiOOH and H_2O. Such a process could account for the slow weight loss discussed above.

In earlier studies [19, 20] on basic nickel carbonates, the endothermic peak at 200°C was attributed to the decomposition of the hydroxide.

However, other studies [3, 21] attributed this to a dehydration process producing an intermediate of composition $NiCO_3 \cdot 3Ni(OH)_2$. The results obtained in the present study from IR analysis and XRD, together with the percentage weight loss, suggest that this process involves both dehydration and initiation of the hydroxide decomposition.

The IR spectrum of the calcination product of THNC at 550°C is given in Fig. 2, curve c. The spectrum shows the complete disappearance of OH^-, H_2O and CO_3^{2-} absorptions, and the presence solely of absorptions at 560, 425 and 300 cm^{-1}, which are assigned to NiO. XRD of this product, given in Fig. 3, in which the 550°C curve displays the typical diffractogram of well crystallized NiO (ASTM card no. 4-835 [17]). Hence, the second weight loss step is associated with the decomposition of the intermediate giving rise to NiO in a fairly crystalline form. This is stable to further heating to 900°C (Fig. 2, curves d, e). This result agrees well with other reported studies [3, 21].

Effect of atmosphere on the decomposition of THNC

The dehydration and the decomposition processes of basic carbonates are not only affected by the type of carbonate, but also by the heating conditions, especially the gas atmosphere used and its pressure [22]. Therefore a separate thermal analysis (TG and DTA) has been conducted on the decomposition of THNC under dynamic atmosphere of dry nitrogen.

The TG and DTA curves, at flow rate of 30 $cm^3\ min^{-1}$ and heating rate of 10 K min^{-1} are shown in Fig. 4. The corresponding curves obtained in dry air and under the same conditions are shown beneath for comparison. The TG curves in both atmospheres are quite similar, with the same weight losses for both stages. However, the relative intensities of the DTA peaks are decreased in nitrogen atmosphere compared to air. This observation is attributed to the occurrence of more than one chemical change in the decomposition.

Non-isothermal kinetic analysis

As previously mentioned, the method proposed by Ozawa [10] was adopted to calculate the kinetic parameters of THNC decomposition.

Table 1 summarizes the characteristics of both stages I and II. Table 1 and Fig. 1 indicate that there is a shift of temperature corresponding to the same weight loss (TG) and peak maxima in the DTA curve due to differences in the heating rate θ. Figure 5 shows this from plots of $\log \theta$ versus $1/T$ constructed from TG curves.

Table 2 shows value of ΔE amounts to 70 kJ mol^{-1} for stage I. This value is higher than that reported for the dehydration of THNC [3]. Such a high value may be attributed to the desorption of physically adsorbed

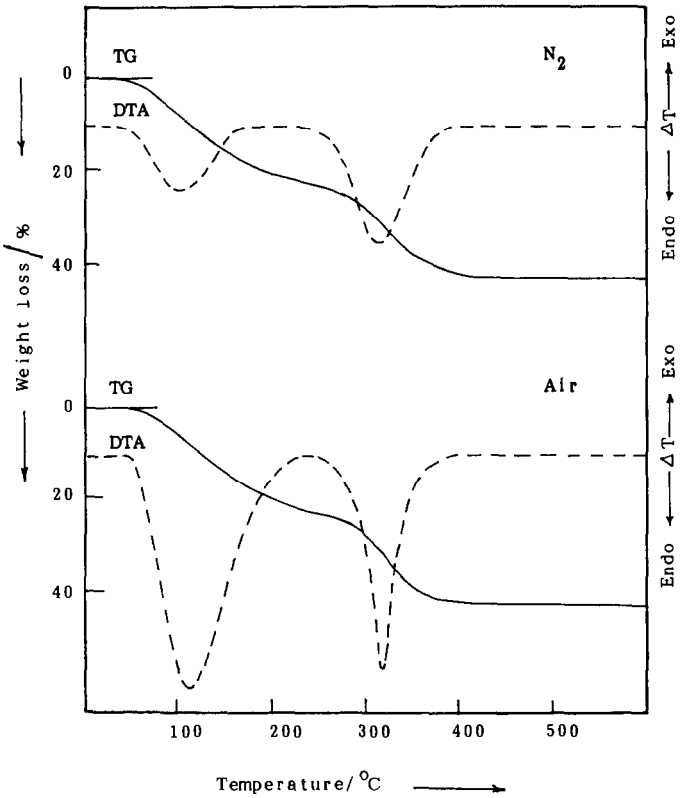

Fig. 4. TG and DTA of THNC at 10 K min^{-1} in dynamic (30 cm^3 min^{-1}) atmosphere of dry nitrogen or air.

TABLE 1

Relationship between the heating rate θ and peak temperature T_{max} of the DTA curves corresponding to stages I and II on the thermal decomposition of THNC [a]

θ	T_{max}		Temperature range	
	I (Endo)	II (Endo)	I	II
2	70	283	35–190	190–350
5	100	300	40–220	220–390
10	115	310	50–225	225–410
20	125	320	60–230	230–420
Weight loss		Obs [b]	21.3	42
		Ant [c]	19.14	40.01

[a] θ in K min^{-1}; T_{max} and temperature range in °C. [b] Observed percentage weight loss. [c] Anticipated percentage weight loss.

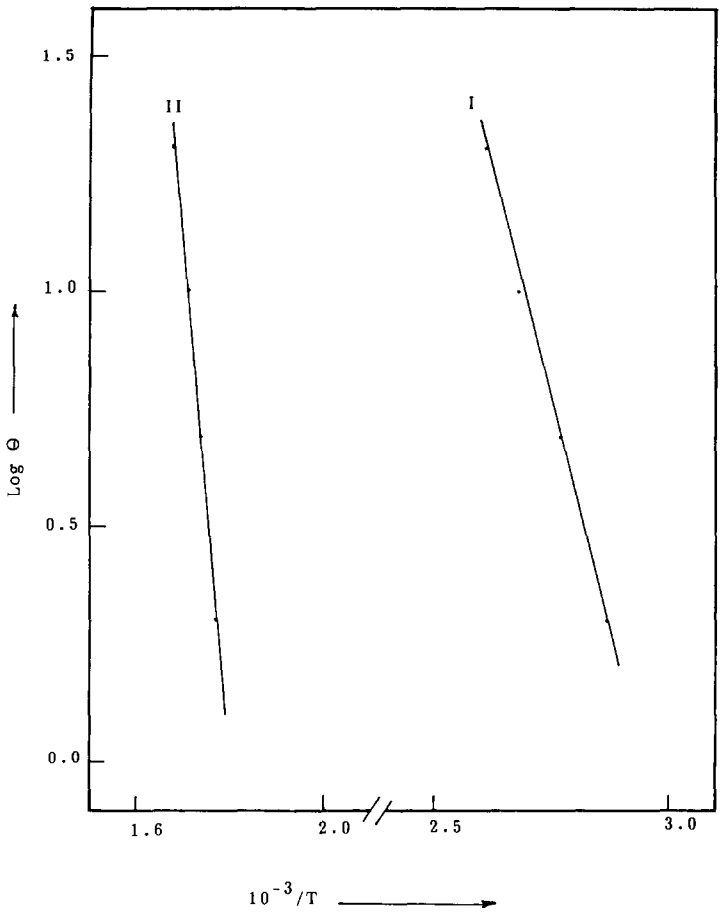

Fig. 5. Plots of log θ vs. $1/T$ for THNC weight loss stages (from the TG curves shown in Fig. 1).

TABLE 2

Non-isothermal kinetic parameters of stages I and II of the thermal decomposition of THNC from TG and DTA data [a]

Stage	ΔE	$k \times 10^{-3}$				log A			
		$\theta = 2$	$\theta = 5$	$\theta = 10$	$\theta = 20$	$\theta = 2$	$\theta = 5$	$\theta = 10$	$\theta = 20$
I	70 ± 3	9.7	22.9	43.3	79.5	8.5	8.49	8.44	8.44
II	190 ± 10	77.8	187.9	363.0	702.2	16.5	16.59	15.58	15.56

[a] ΔE in kJ mol^{-1}; k in min^{-1}; θ in K min^{-1}.

TABLE 3

Non-isothermal kinetic and thermodynamic parameters [a] of stages I and II of the thermal decomposition of THNC from DSC measurements based on $\theta = 10\,K\,min^{-1}$

Stage	Temperature range	ΔE	$\ln A$	k	ΔH	C_p	ΔS	Characterization
I	131–260	47 ± 2	12.8	0.347	141.8	1.948	1.087	Endo
II	278–394	112 ± 2	20.56	0.349	49.62	1.222	0.250	Endo

[a] Temperature range in °C; ΔE and ΔH in kJ mol^{-1}; k in min^{-1}; C_p in J g^{-1}; ΔS in J K^{-1} g^{-1}.

water involved in stage I, since the range of ΔE characterizing such physisorption process is about 60 kJ mol^{-1}. Furthermore, the activation energy could include some early dissociation of the $Ni(OH)_2$ to NiOOH phase.

The activation energy ΔE calculated for the second stage was 190 kJ mol^{-1}, see Table 1. This value corresponds to the decomposition and elimination of CO_2 and H_2O. It has been stated earlier that the overall rate of THNC decomposition is controlled by the rate at which the gaseous components can diffuse away from the reaction centre [23]. One could suggest that the rapid and effectively complete withdrawal of CO_2 and H_2O from the reaction medium, as well as the occurrence of the decomposition of $NiCO_3$, $Ni(OH)_2$ and NiOOH species in the same event, may increase the difficulty of such gaseous evolution. These effects could account for the high value of the calculated activation energy ΔE.

The kinetic and thermodynamic parameters of the two stages in the thermal decomposition of THNC in nitrogen are summarized in Table 3. Figure 6 shows DSC curves recorded at different heating rates ($\theta = 2$, 5, 10 and 20 K min^{-1}). Plots of $\log \theta$ versus $1/T$, constructed from these curves, are given in Fig. 7.

Figure 6 displays two endothermic peaks, the first one has a shoulder at low temperature corresponding to the first stage in the decomposition of THNC. This is more obvious at higher heating rates (5, 10 and 20 K min^{-1}). The peak shape supports the proposition that desorption of physisorbed water, the elimination of water of crystallization and the beginning of the decomposition of $Ni(OH)_2$ are involved. The activation energy ΔE and the enthalpy change ΔH for this process are 47 and 141.8 kJ mol^{-1}, respectively. Such high values are consistent with the many steps involved. The difference in activation energies from those listed in Table 2 may be due to the change in the atmosphere (from air to nitrogen).

The activation energy for the second endothermic peak is 112 kJ mol^{-1}. This value agrees well with that obtained by Dollimore and Taylor [4] under the same conditions (nitrogen atmosphere). The low value for ΔS could be understood from the highly crystalline nature of NiO (XRD). ΔE values obtained from the DSC measurements are less than those

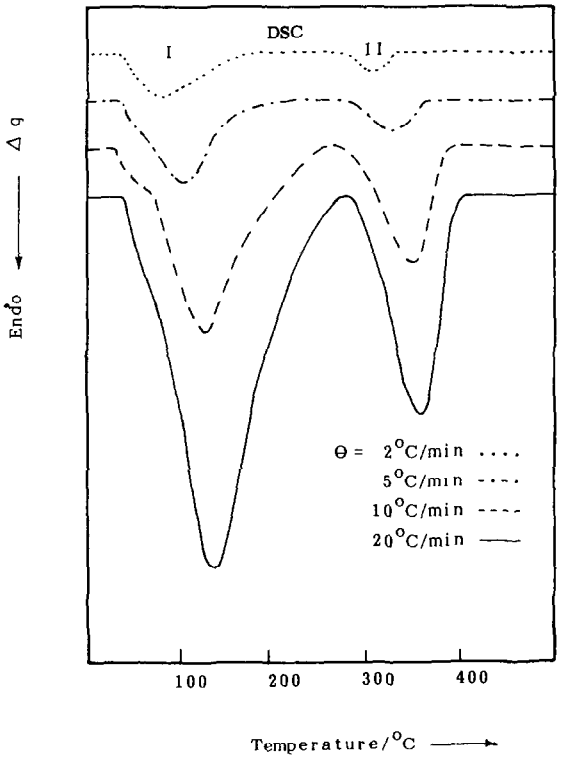

Fig. 6. DSC of THNC at the heating rates (θ) indicated and in dynamic (30 $cm^3 min^{-1}$) atmosphere of dry nitrogen. Stages I and II are indicated.

calculated from TG and DTA curves in air. However the former are closer to those reported for these processes.

This comparative study confirms the idea that such endothermic reactions may be sensitive to the atmosphere [3, 22], and the reaction conditions [5]. Moreover, non-isothermal kinetic parameters calculated from DSC results are in good agreement with the reported data from isothermal studies.

Electron microscopic examinations

SEM of the parent THNC revealed a wide range of crystals sizes. The material looked like an agglomerate more than separate crystals. Figure 8 shows a typical crystal of the reactant exhibiting a smooth edge; however it was fractured. The fine powder suggests the presence of amorphous material rather than the large crystal. These observations agree with the XRD results which show an amorphous structure for the reactant THNC (Fig. 3).

Samples heated to 150°C (Fig. 9), corresponding with the start of the

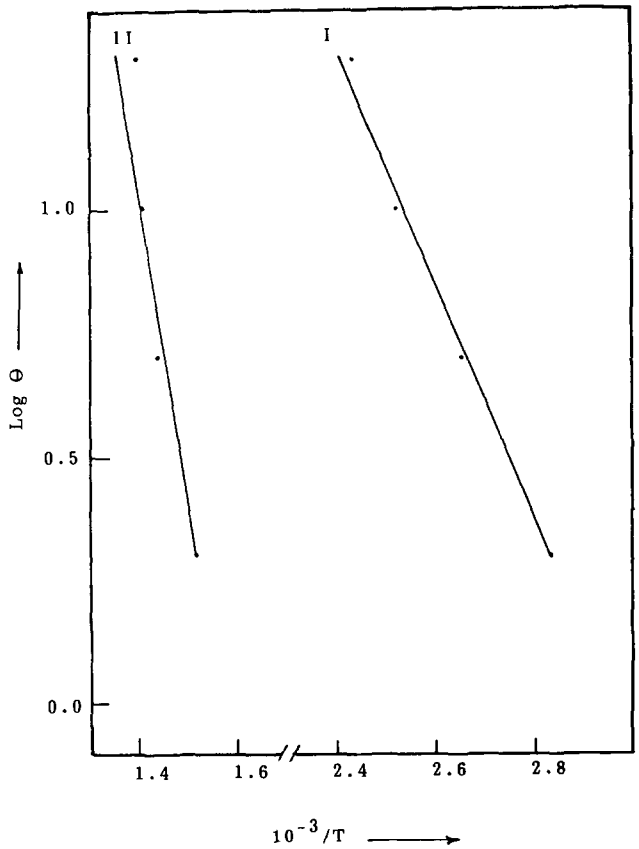

Fig. 7. Plots of log θ vs. $1/T$ from the DSC of THNC. (Fig. 6).

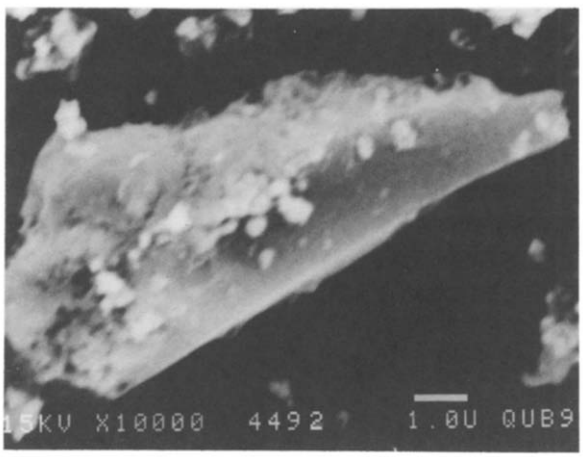

Fig. 8. Scanning electron micrograph of THNC.

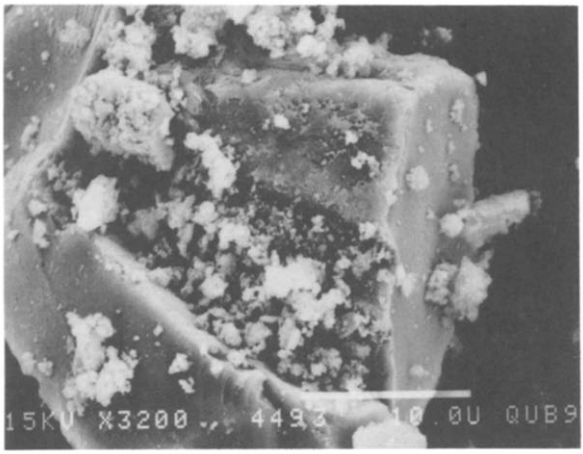

Fig. 9. Scanning electron micrograph of THNC heated to 150°C corresponding to the start of the dehydration process.

dehydration process, show the formation of finely-divided texture with fragmented layer crystallites. Such features are increased at 220°C, Fig. 10. The dehydration process appeared to spread and penetrate into the bulk of the crystals resulting in an increase in the amorphous nature of the material, an observation which was confirmed by the X-ray diffraction studies (Fig. 3).

Further heating to 320°C resulted in the appearance of the decomposition products as nodules (Fig. 11(a)). Figure 11(b) illustrates the extensive crystal disruption accompanying the progress of the decomposition process. The individuality of the reactant particles was maintained to a small extent, but the basal plane faces were extensively perforated.

The final decomposition product obtained at 550°C (Fig. 12) were

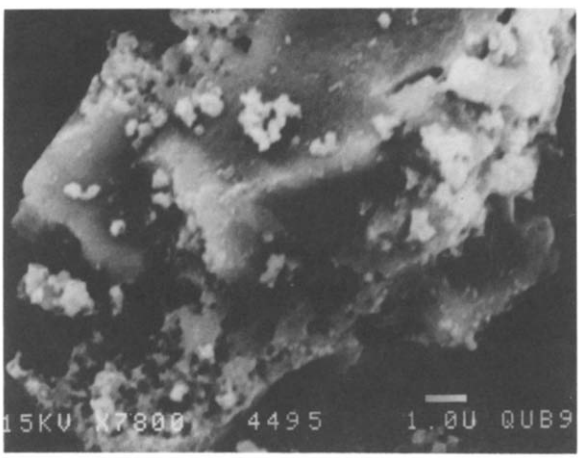

Fig. 10. Scanning electron micrograph of THNC calcined at 220°C.

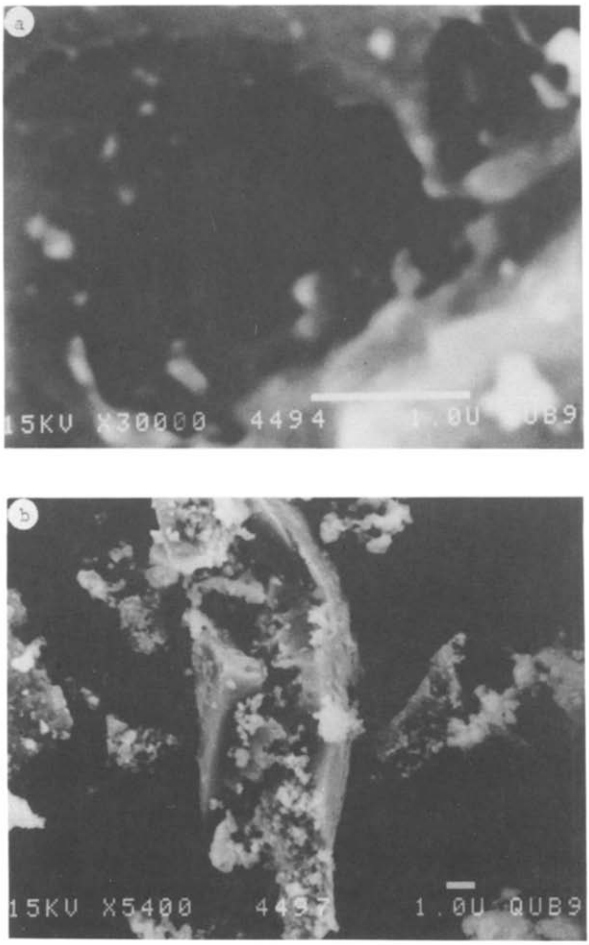

Fig. 11. Scanning electron micrograph of THNC: (a) heated to 320°C corresponding to the start of decomposition; (b) calcined at 320°C for 2 h corresponding to the progressive increase in decomposition.

pseudomorphic with the original THNC. Such product particles comprised aggregates of small adherent particles. XRD (Fig. 3) indicates that this material is highly crystalline NiO. Hence it could be concluded that calcination of THNC produces very fine NiO cyrstals.

CONCLUSIONS

The thermal decomposition of tetrahydroxy basic nickel carbonate occurs by two steps, dehydration and decomposition. However, the dehydrated intermediate undergoes a topochemical reaction resulting in the formation of NiOOH. Crystalline nickel oxide (NiO) is obtained at 500°C. The decomposition mechanism in air can be presented as

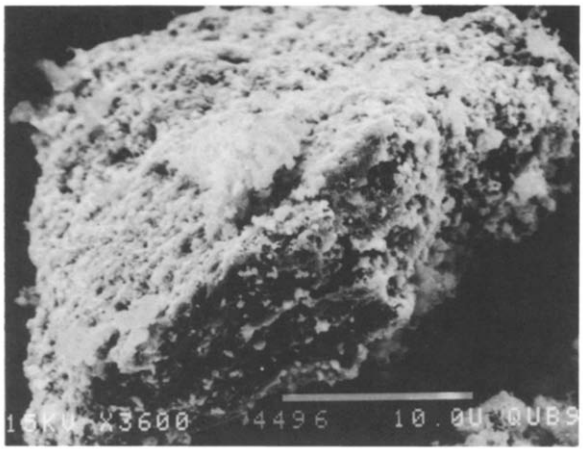

Fig. 12. Scanning electron micrograph of the completely decomposed crystal of THNC.

$$2[NiCO_3 \cdot 2Ni(OH)_2 \cdot 4H_2O] \longrightarrow 2[NiCO_3 \cdot 2Ni(OH)_2] + 8H_2O$$

$$\downarrow +0.5O_2 \text{ (from air)}$$

$$2NiCO_3 \cdot 2Ni(OH)_2 \cdot 2NiOOH + H_2O\uparrow \quad (7)$$

$$2NiCO_3 \cdot 2Ni(OH)_2 \cdot 2NiOOH \longrightarrow 6NiO + 2CO_2 + 6H_2O + 0.5O_2\uparrow \quad (8)$$

Additionally one can conclude that the kinetic study of the decomposition of solids is better understood when complementary investigations on the chemical nature of intermediates and the products are carried out. This confirms the viewpoint of Galwey [11] who stated that the interpretation of kinetic data should be supported by all other available and relevant evidence, and more chemical approaches should be considered in reactions involving solids.

ACKNOWLEDGEMENTS

It is a pleasure to thank the Queen's University of Belfast, particularly the staff of the Electron Microscope Unit for assistance in obtaining the electron micrographs. Thanks are also due to the Egyptian Government for the grant of a Fellowship.

REFERENCES

1 H. Henmi, T. Hirayama, N. Mizutani and M. Kato, Thermochim. Acta, 96 (1985) 145.
2 N.A. Carthrey, D.H. Kerridge and S.A. Tariq, Thermochim. Acta, 61 (1983) 185.
3 R.M. Gabr, M.M. Girgis and A.M. El-Awad, Thermochim. Acta, 196 (1992) 279.
4 D. Dollimore and T.J. Taylor, Thermochim. Acta, 40 (1980) 279.
5 H. Henmi, M. Mori, T. Hirayama, N. Mizutani and M. Kato, Thermochim. Acta, 104 (1986) 101.

6 D.I. Trimm, Design of Industrial Catalysts, Chemical Engineering Monographs, Vol. 11, Elsevier, Amsterdam, 1980.
7 J.H. Flyn and L.A. Wall, J. Res. Natl. Bur. Stand., Sect. A, 70 (1966) 487.
8 W.E. Brown, D. Dollimore and A.K. Galwey, in C.H. Bamford and C.F.H. Tipper (Eds.), Reactions in the Solid State, Chemical Kinetics, Vol. 22, Elsevier, Amsterdam, 1980, pp. 99–109.
9 N.D. Topor, L.I. Tolokhnikova and B.M. Kadenatsi, J. Therm. Anal., 22 (1981) 221.
10 T. Ozawa, J. Therm. Anal., 2 (1970) 301.
11 A.K. Galwey, React. Solids, 8 (1990) 211.
12 R.C. Weast (Ed.), Handbook of Chemistry and Physics, 57th edn., CRC Press, New York, 1976.
13 A.A. Duswalt, Thermochim. Acta, 8 (1974) 57.
14 Gyulai and E.J. Greenhow, Talanta, 21 (1974) 131.
15 K.F. Baker, Thermal Analysis Application Brief, No. TA-53, Du Pont Instruments, Wilmington, DE.
16 C. Heald and A.C.K. Smith, Applied Physical Chemistry, Macmillan, London, 1982, pp. 20–40.
17 W. Frank et al. (Eds.), Power Diffraction File for Inorganic Phase, Int. Center for Diffraction Data, Philadelphia, PA, 1981.
18 J.A.Gadsden, Infrared Spectra of Minerals and Related Inorganic Compounds, Butterworth, London, 1975.
19 C.W. Beck, Thesis, Harvard University, Cambridge, MA, 1964.
20 J. Francois-Rossetti, M. Charton and B. Imelik, Bull. Soc. Chim. Fr., (1957) 614.
21 R.M. Mayalla and A.R. Murthy, J. Indian Inst. Sci., 43 (1961) 87.
22 H. Henmi, T. Hirayama, S. Shanmugarajeh, N. Nizutani and M. Kato, Thermochim. Acta, 106 (1986) 263.
23 P.D. Garn, in H. Kambe and P.D. Garn (Eds.), Thermal Analysis, Academic Press, New York, 1970, p. 100.